Scripta Materialia 129 (2017) 20–24

Contents lists available at ScienceDirect

Scripta Materialia

journal homepage: www.elsevier.com/locate/scriptamat

Regular Article

Tailoring the morphology in Y_2O_3 doped melt-grown Al_2O_3/ZrO_2 eutectic ceramic

Liansheng Fu [a], Xuesong Fu [a], Guoqing Chen [a,*], Wen-bo Han [b], Wenlong Zhou [a]

[a] School of Materials Science and Technology, Dalian University of Technology, Dalian 116085, PR China
[b] National Key Laboratory of Science and Technology on Advanced Composites in Special Environment, Harbin Institute of Technology, Harbin, 150080, PR China

ARTICLE INFO

Article history:
Received 29 August 2016
Received in revised form 11 October 2016
Accepted 19 October 2016
Available online 27 October 2016

Keywords:
Eutectic ceramic
$Al_2O_3/ZrO_2(Y_2O_3)$
Crystal growth
Constitutional supercooling

ABSTRACT

The addition of more components are an interesting way of the microstructural controls. Herein, adding Y_2O_3 to Al_2O_3-ZrO_2 bulk eutectic at the low G/v ratio (thermal gradient G divided by growth rate v) was adopted to tailor the morphology. As the Y_2O_3 content increases, the solidification structure changes obviously from cellular into the dendritic shape. Especially, a typical irregular $Al_2O_3/ZrO_2/Y_3Al_5O_{12}$ (YAG) ternary eutectic appeared in the inter-colony region for the higher Y_2O_3 content. This microstructure transition is consistent with the classical constitutional supercooling criterion.

Eutectic oxide ceramics prepared by the solidification from the melts exhibit excellent mechanical properties, thermal stability, and oxidation resistance in atmosphere at high temperature. Therefore, they are considered appropriate candidates for ultra-high-temperature materials for aerospace, jet aircraft engine, and gas turbine system applications [1–4]. In particular, binary and ternary eutectics of the Al_2O_3-ZrO_2-Y_2O_3 system are marked because of their outstanding mechanical properties with a remarkable strength retention up to nearly the melting temperature and a suitable thermal shock resistance [5–7].

The mechanical properties of Al_2O_3-based eutectic composite depends strongly on its microstructure. Higher strength could be achieved by refining the microstructure with the reducing of the flaw sizes [7–10]. Enhancing the growth rates of the melt is the most effective way to reduce the size of the eutectic domains [1,11–13]. Addition of more components is another important strategy to further manipulate the eutectic microstructure. The addition of more components to the eutectic system may decrease the growth length scales to produce finer structures [7,14,15]. Furthermore, recent reports showed that adding components could be used to amend the bonding interface, which will enhance the toughness [16,17].

In Al_2O_3-ZrO_2-Y_2O_3 system, adding Y_2O_3 to Al_2O_3-ZrO_2 eutectic were widely studied previously [18]. For Al_2O_3/ZrO_2 system which can accept high amount of yttrium, the Y_2O_3 addition led to the pseudo-binary eutectic in which various zirconia polymorphs (monoclinic, tetragonal or cubic zirconia) could be obtained just by changing the Y_2O_3 content. The presence of the zirconia polymorphs gave rise to a rich variety of microstructural morphologies and residual stress states, which controlled the mechanical properties [18–20]. Previous investigations have reported the eutectic composition with 1 mol% Y_2O_3 addition presented the highest strength at room temperature [18,21,22]. Some other studies show that apart from the growth rate, Y_2O_3 addition can also have an effect on the appearance of eutectic structure, such as lamellar, Chinese-script and rod-like structures [23]. Lee et al. [24] found out the eutectic microstructure changed dramatically with the growth rate, and the morphology and the rate of transformation were affected by the amount of Y_2O_3. Farmer et al. [22] discovered that Y_2O_3 addition may give rise to colony structure easily, and the colony size decreases as Y_2O_3 increases. The colony structure as a typical microstructure in the Al_2O_3-$ZrO_2(Y_2O_3)$ eutectic system has an important influence on its mechanical properties. However, there are few research concerned the control of the colony morphological characteristics.

In this work, the melt-grown Al_2O_3-$ZrO_2(Y_2O_3)$ eutectic ingots with different Y_2O_3 contents were grown to investigate the effect of Y_2O_3 concentration on the microstructure development at the low G/v ratio (thermal gradient divided by growth rate). Furthermore, the formation and transition mechanism of the colony structure with the doping amount of Y_2O_3 were also analyzed.

The raw material was prepared using a mixture of commercial nanopowders with average grain size of 50 nm of Al_2O_3 (99.99%), Y_2O_3 (99.99%), and ZrO_2 (99.99%), and contained 63 mol% Al_2O_3 and 37 mol% of a mixture of ZrO_2 and Y_2O_3 corresponding to the eutectic composition which has been formulated according to the phase diagram given by Lakiza and Lopato [25]. The different specimens with

* Corresponding author at: School of Materials Science and Engineering, Dalian University of Technology, No. 2, Linggong Road, Dalian 116085, PR China.
E-mail address: gqchen@dlut.edu.cn (G. Chen).

http://dx.doi.org/10.1016/j.scriptamat.2016.10.024
1359-6462/

six nominal Y_2O_3 contents were prepared, and the corresponding proportions of Y_2O_3 in relation to the total $ZrO_2 + Y_2O_3$ content (expressed by Y = mol% Y_2O_3 / (mol% ZrO_2 + mol% Y_2O_3)) were 0, 1.5%, 3%, 4.5%, 8%, and 12%, designated as 0Y, 1.5Y, 3Y, 4.5Y, 8Y, and 12Y, respectively.

The powders were mixed and dissolved thoroughly in the alcohol by electromagnetic stirring and ultrasonic wave shaking at room temperature to obtain a homogeneous slurry. The mixed powders was dried at 80 °C in air, and then hand-milled in an agate mortar. Precursor powders were calcined in air at 1000 °C for 1 h. Precursor rods of 20 mm diameter × 10 mm were prepared from the nanocomposite powders by hot pressing sintering method in graphite die at 1450 °C for 1 h under 30 MPa to get high-density (>98%) precursors. The as-sintered rod was then melted in Mo molds in a furnace equipped with a graphite heater. The eutectic temperature of 1862 °C was slightly decreased as the doping amount of Y_2O_3 was increased, so the melt was heated to 1950 °C, and held for 60 min in a high-purity argon atmosphere chamber. Melt was then cooled down to 1870 °C, held for 5 min to equilibrate the temperature, and finally solidified to room temperature at a cooling rate of 10 °C/min.

The as-solidified rods were cut with a diamond saw and the cross-sections were polished with diamond paste up to 1.5 μm. The polished surfaces were coated with a thin layer of Au before observation. The microstructure and component phases of the composites were determined by scanning electron microscopy (SEM), electron probe microanalysis (EPMA), energy disperse spectroscopy (EDS, Link-Isis) and X-ray diffraction techniques (XRD).

Fig. 1 shows the cross-sectional microstructures in the central area of $Al_2O_3/ZrO_2(Y_2O_3)$ melt-grown eutectic ingots doped different Y_2O_3 contents of 0Y, 1.5Y, 3Y, 4.5Y, 8Y, and 12Y. The eutectic microstructure of all samples was composed of a typical colony structure. The center of each colony was composed of an Al_2O_3 matrix (dark areas) containing a regular distribution of white zirconia fibers of ≈0.1 μm order of magnitude in diameter (insets in Fig. 1(a) and (c)) or a disordered interpenetrating network of fine ZrO_2 lamellae (inset in Fig. 1(f)). This microstructure characteristic was consistent with the results obtained by Pastor et al. [26], in which the specimens were prepared by the laser-heated floating zone method. The average interphase spacing in the colonies decreases from 1.8 μm for 0Y to 1.1 μm for 3Y with increasing Y_2O_3 content, then increases slightly, as the insets of (a), (c) and (f) 12Y shown in Fig. 1. The colony core was surrounded by a thick intercolony region formed by coarse ZrO_2 particles with the irregular shape. X-ray diffraction patterns showed that the crystal structures of the ZrO_2 phase changed from monoclinic for 0Y, monoclinic and tetragonal for 1.5Y and 3Y, tetragonal and cubic for 4.5Y to cubic for up to 8Y by the Y_2O_3 addition. However, an alumina-yttria-rich phase (gray color) was identified in this inter-colony region, as shown in Fig. 1(f), which was assigned to the yttrium aluminum garnet (YAG) phase.

Furthermore, it should be noted that a typical irregular 'Chinese script' Al_2O_3/ZrO_2/YAG ternary eutectic microstructure appeared occasionally in the inter-colony region of the 12Y sample, as the C region shown in Fig. 2(a), which is similar to that of the directionally solidified Al_2O_3/ZrO_2/YAG prepared by the directional solidification reported by

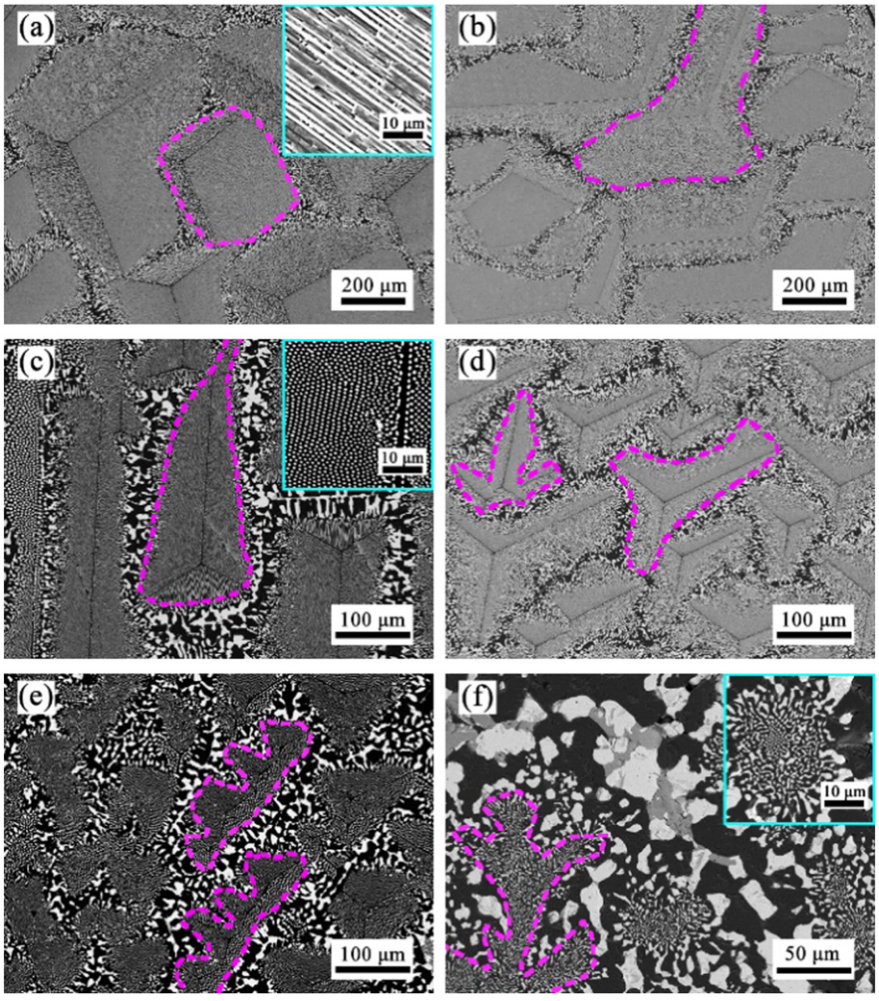

Fig. 1. Back scattered electron images of (a) 0Y, (b) 1.5Y, (c) 3Y, (d) 4.5Y, (e) 8Y, and (f) 12Y eutectic ceramic bulks at the cooling rate of 10 °C/min (insets of (a) 0Y, (c) 3Y and (f) 12Y samples show an enlarged portion of the well-ordered and disordered regions, respectively). The black, white and gray contrasts correspond to a-Al_2O_3, ZrO_2 and YAG phases, respectively.

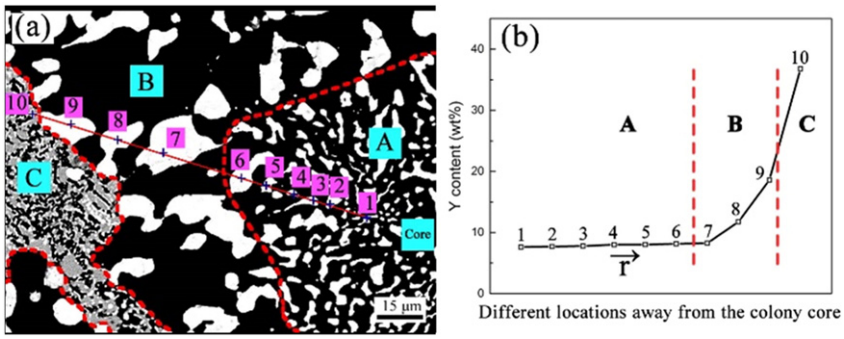

Fig. 2. (a) Back scattered electron image of the colony in 12Y sample: A region showing the disordered interpenetrating network microstructures of the colony structure surrounded by the B and C regions; B region showing the coarse ZrO_2 particles of irregular shape in the inter-colony regions; C region showing a typical irregular 'Chinese script' Al_2O_3/ZrO_2/YAG ternary eutectic microstructure in the inter-colony regions; (b) Y_2O_3 concentrations in the ZrO_2 phase along the cross-section radius direction (r direction) of the colony on the red solid line in (a) analyzed by EPMA.

Nagira et al. [27]. The corresponding EPMA results of the Fig. 2(a) are given in Fig. 2(b). The yttrium concentration increases along with the radius direction (r direction), and the ZrO_2 phase in the inter-colony region (B region) gives a sharply higher yttrium content than that in the colony (A region), which indicates that the segregation of yttrium occurred during the solidification. When the higher Y_2O_3 content enrichment in the intercolony region exceeds the solubility of ZrO_2 phase, it will make the composition lie close to the boundary of the Al_2O_3-ZrO_2-$Y_3Al_5O_{12}$ phase field, which led to the formation of the irregular Al_2O_3/ZrO_2/YAG ternary eutectic microstructure.

It can be seen that the colony size decreases and intercolony area increases with the increase of Y_2O_3 content. Furthermore, the geometrical shape of the $Al_2O_3/ZrO_2(Y_2O_3)$ eutectic colony morphology also changed dramatically with the increase of the Y_2O_3 content. When adding a small amount of the Y_2O_3 stabilizer (<3 mol%, with respect to zirconia), the colony morphology exhibited sub-rounded or ellipsoidal cellular shape, as shown in Fig. 1(a–c). Sometimes a modicum of grooves formed along colony boundary of the 1.5Y and 3Y samples. When the Y_2O_3 content was enhanced to 4.5 mol%, the massive grooves appeared, as shown in Fig. 1(d). As the Y_2O_3 content was at the 8 mol%, the colony with serrated cellular dendritic shape appeared in Fig. 1(e). When the Y_2O_3 content further increased up to 12 mol%, the morphology characteristic of colony turned into the dendritic form, as shown in Fig. 3(f). This obvious transition of the colony morphology with the increase of Y_2O_3 content can be elucidate by the constitutional supercooling criterion similar to the solidification behavior of the impure metals and metallic alloys.

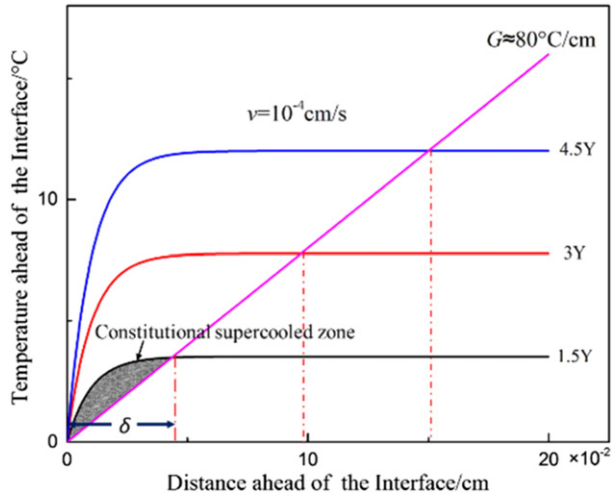

Fig. 3. Equilibrium liquidus temperature, calculated from Eq. (3) at different C_0, and specimen temperature (straight line) calculated from Eq. (4), as functions of distance ahead of the interface. The shadow area showing the constitutional supercooled zone, in which the δ represents the nominal length of the constitutional supercooled zone.

Constitutional supercooling has been described and discussed qualitatively [28]. The length δ of the constitutionally supercooled zone may be calculated by comparing the equilibrium temperature distribution with the temperature gradient for any point in front of the interface.

For the steady-state growth of an interface, the equilibrium temperature for any point in front of the interface was given by

$$T_L = T_m - mC_0\left[1+\frac{1-k}{k}\,exp\left(-\frac{\nu x}{D}\right)\right] \tag{1}$$

where T_m is the melting point of the pure metal, m is the slope of the liquidus line and assumed to be constant for simplicity, ν is the growth rate of the crystal, k is the equilibrium segregation coefficient, C_0 is the impurity concentration in the melt, D is the diffusion coefficient of the impurity in the melt, and x is the distance measured from the interface into the liquid.

The temperature gradient in front of the interface may be expressed as

$$T = T_m - m\frac{C_0}{k} + Gx \tag{2}$$

where $T_m - m\frac{C_0}{k}$ is the temperature at the interface, and G is the temperature gradient in the liquid.

If the above Eqs. (1) and (2) are plotted, the point of intersection other than $x=0$ will give the length δ of the supercooled zone. Thus, for $T=T_L$, it can be obtained that

$$1-\exp\left(-\frac{\nu x}{D}\right) = \frac{G}{mC_0(1-k)/k}x \tag{3}$$

The length δ of the supercooled zone depends strongly on the growth rate ν, the solidification thermal gradient G and the solute concentration C_0. Herein, ignoring the kinetic undercooling in this stage, we assumed the Al_2O_3/ZrO_2 binary eutectic melt as the pure metal melt during solidification, and the Y_2O_3 addition can be deemed as the impurity. In this study, the growth rate v was calculated according to $\lambda = 1\times\nu^{-1/2}\ \mu m^{1.5}\ s^{-0.5}$ [29]. Ignoring the Y_2O_3 content on the growth rate, we approximately took $\lambda\approx 1\ \mu m$ as the average interphase spacing (see the insets in Fig. 1) for the calculation. The growth rate $\nu = 1\times10^{-4}$ cm/s was obtained, eventually. Based on Eq. (3), we took the thermal gradient $G =$ °C/cm (<10^2 °C/cm [19]) for example to qualitatively calculate the nominal length δ variation of the supercooled zone for different Y_2O_3 content C_0. The approximate physical parameters are shown in Table 1.

Table 1
Physical parameters used for the calculation.

Parameters	Values	Reference
D (cm^2/s)	1×10^{-6}	[30] approx.
$\bar{k}$	0.58	[31] calc.
$\bar{m}$ (°C/mol%)	9.75	[25] calc.

The discrimination of constitutional supercooling has been theoretically proposed as follows:

$$G < \left(\frac{dT_L}{dx}\right)_{x=0} \tag{4}$$

The Eq. (4) can be further written as

$$\frac{G}{v} < \frac{mC_0}{D}\frac{1-k}{k} \tag{5}$$

According to Eq. (5), one can determine the formation of cellular or dendrite structure strongly depends on the growth rate v, the solidification thermal gradient G, and the solute concentration C_0.

Although the growth rate in this study was very low ($v \approx 1 \times 10^{-4}$ cm/s), the colony structures with sub-rounded cellular geometric shape in 0Y sample without Y_2O_3 dopant were also observed in Fig. 1(a). This was different from that prepared by the laser-heated floating zone (LHFZ) method under the relatively high growth rate ($v = 20$ mm/h), in which a homogeneous dispersion of irregular ZrO_2 lamellae within the Al_2O_3 matrix was obtained in the small-dimension rods of 1.2–1.6 mm in diameter [26]. This is due to that the LHFZ method can produce higher thermal gradient (10^4 K/cm [19]) in the small-dimension samples, which will keep the solid-liquid interfaces flat during growth. However, large-size samples (radius $R = 10$ mm) prepared by conventional casting method in this study would generate a relatively low-temperature gradient G (<10^2 °C/cm [19]) in the melt [32], in which the resulted small G/v ratio may meet the conditions of Eq. (5) to lead to the break-down of planar growing interface to generate a cellular or dendritic structure. However the cellular eutectic growth with a revolution paraboloid tip interface happened in the melt of the 0Y sample. The significant concentration difference between the two eutectic phases may reduce the growth velocity considerably. So the thermal field around the adjacent cells overlapped severely to restrain the lateral branching of the cellular interface and sub-rounded cellular eutectics formed.

As the Y_2O_3 was added, the solidification interface morphology was also controlled by its longitudinal diffusion. This may create another solute field superposed around the advancing eutectic dendrite tip. To diffuse away the enriched Y_2O_3 solute easily, the tip radius decreases with the increase of Y_2O_3 content, as shown in Fig. 1. Eqs. (1) and (2) were plotted in Fig. 3. The graph gives the nominal length δ of the supercooled zone for different Y_2O_3 content (C_0). As the Y_2O_3 content increased, the supercooled zone length δ become much larger. This will result in a different solidification behavior, which made the interface morphology obviously change from a cellular shape into the dendritic form with the increase of Y_2O_3 content.

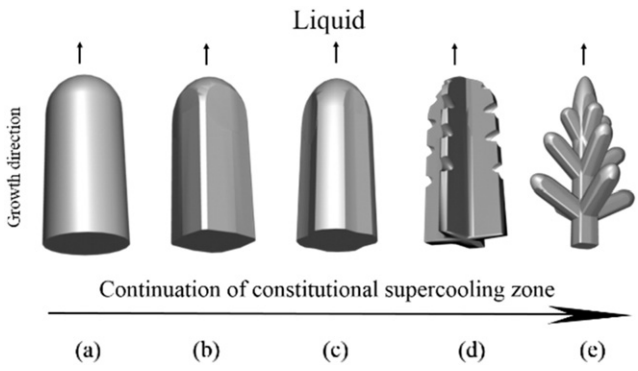

Fig. 4. Schematic diagram of colony shape evolution versus the scale of constitutional supercooling zone.

Based on the above results, an evolution model of the interface shape as a function of the Y_2O_3 content was considered, as shown in Fig. 4. At first, the colony shape of 0Y sample without the Y_2O_3 addition in Fig. 1(a) reflected that its growth cellular interface was sub-rounded column in this experiment, as shown in Fig. 4(a). The Y_2O_3 addition yielded an additional constitutional undercooling ahead of the advancing solid/liquid interface, as the shadow area shown in Fig.3. This may destabilize the original cellular interface. The crystal growth direction can transform into other preferential orientations and generate some protrusion penetrating to the melt further, which was controlled by the length of constitutionally supercooled zone. Details are as follows:

A small amount of Y_2O_3 addition produced a narrow constitutional supercooled zone. This made the sub-rounded cellular interface initiate small-amplitude transverse growth to form an ellipsoidal interface (Fig. 4(b)). This was parallel to colony morphologies as shown in Fig. 1(b) and (c). Sometimes a handful of grooves formed along colony boundary, where the interface was retarded by large-size yttrium atoms. When Y_2O_3 content increased, obvious protrusions or pits were then generated in the cellular interface due to the continuation of constitutional supercooling, as shown in Fig. 4(c), which corresponded to 4.5Y sample shown in Fig. 1(d). As Y_2O_3 content further increased, the serrated cellular dendritic interface presented schematically in Fig. 4(d) is shown in Fig. 1(e). When the Y_2O_3 content was large enough, substantial constitutionally supercooled zone was obtained in the melt. This may render the cellular protrusions penetrating to the melt further and initiated large-amplitude lateral growth, which led to the formation of dendritic interface, as shown in Fig. 4(e). And the 12Y sample shown in Fig. 1(f) was the corresponding example. However, once dendrites formed, the most may quickly become highly unstable because of all the surface area they possess. One way to reduce the surface area is by causing the dendrite arms to "melt" or dissolve off completely. The convection process may carry the remelted dendrite arm somewhere else where it can grow to a new equiaxed randomly oriented cellular colony microstructure, as shown in Fig. 1(f). Besides, when the constitutional supercooling was large enough, the grains of the solid can also nucleate in the melt ahead of the solid-liquid interface. This was completely different from that of the specimens with the same composition prepared by the laser-heated floating zone method (LFZ) reported by Pastor et al. [26]. Pastor obtained three different microstructures (the lamellae, colonies and elongated cells) depending on the growth rate. This evident difference comes from the great disparity in the apparent thermal gradient. The growth thermal gradients of up to 10^4 K/cm can be obtained by LFZ method [19], in which the larger G/v ratio may produce the smaller constitutionally supercooled zone to limit the branch growth. Therefore, Y_2O_3 addition may affect the growth interface morphology of melt-grown Al_2O_3-ZrO_2 eutectic bulks, remarkably.

In summary, Al_2O_3/ZrO_2 eutectic bulks 20 mm in diameter containing various amounts of the Y_2O_3 were grown by the melt-grown method. The Y_2O_3 content had a pronounced effect on the microstructure morphology at the low G/v ratio (thermal gradient divided by growth rate).

The eutectic ceramic microstructure of samples with different Y_2O_3 addition composed of a typical randomly-orientated colony structure with various geometrical shapes surrounded by a thick intercolony region formed by coarse particles of irregular shape. The colony size decreases and intercolony area increases as the Y_2O_3 content increases. Furthermore, the geometrical shapes of the colony morphology also changed from a sub-rounded cellular to ellipsoidal cellular with protrusions or pits, the serrated cellular, and then to dendritic form, respectively, which was analyzed by the constitutional supercooling criterion

similar to the solidification behavior of the impure metals or alloys. And this microstructure evolution was attributed to the enlarging of a constitutionally supercooled zone of the melt just ahead of the interface with the increase of Y_2O_3 content on cooling. Therefore, the colony morphology in eutectic ceramics can be tailored by the Y_2O_3 addition.

Acknowledgement

This work was supported by the National Natural Science Foundation of China under grant numbers 51675078, 51175059 and 50875032.

References

[1] G. Chen, X. Fu, J. Luo, Y. Zu, W. Zhou, J. Eur. Ceram. Soc. 32 (2012) 4195–4204.
[2] J.M. Calderon-Moreno, M. Yoshimura, J. Eur. Ceram. Soc. 25 (2005) 1365–1368.
[3] Y. Harada, N. Uekawa, T. Kojima, K. Kakegawa, J. Eur. Ceram. Soc. 28 (2008) 1973–1978.
[4] L. Mazerolles, L. Perriere, S. Lartigue-Korinek, N. Piquet, M. Parlier, J. Eur. Ceram. Soc. 28 (2008) 2301–2308.
[5] M.C. Mesa, P.B. Oliete, R.I. Merino, V.M. Orera, J. Eur. Ceram. Soc. 33 (2013) 2587–2596.
[6] J.Y. Pastor, J. Llorca, A. Salazar, P.B. Oliete, I. de Francisco, J.I. Pena, J. Am. Ceram. Soc. 88 (2005) 1488–1495.
[7] P.B. Oliete, J.I. Peña, A. Larrea, V.M. Orera, J. Llorca, J.Y. Pastor, A. Martín, J. Segurado, Adv. Mater. 19 (2007) 2313–2318.
[8] M.C. Mesa, S. Serrano-Zabaleta, P.B. Oliete, A. Larrea, J. Eur. Ceram. Soc. 34 (2014) 2071–2080.
[9] V.M. Orera, R.I. Merino, J.A. Pardo, A. Larrea, J.I. Peña, C. González, P. Poza, J.Y. Pastor, J. Llorca, Acta Mater. 48 (2000) 4683–4689.
[10] X.-s. Fu, G.-q. Chen, Y.-f. Zu, J.-t. Luo, W.-l. Zhou, Ceram. Int. 39 (2013) 7445–7452.
[11] M.C. Mesa, P.B. Oliete, V.M. Orera, J.Y. Pastor, A. Martín, J. Llorca, J. Eur. Ceram. Soc. 31 (2011) 1241–1250.
[12] J.H. Lee, A. Yoshikawa, T. Fukuda, Y. Waku, J. Cryst. Growth 231 (2001) 115–120.
[13] F.A. Huamán-Mamani, M. Jiménez-Melendo, M.C. Mesa, P.B. Oliete, J. Alloys Compd. 536 (2012) S527–S531.
[14] M.C. Mesa, P.B. Oliete, J.Y. Pastor, A. Martín, J. Llorca, J. Eur. Ceram. Soc. 34 (2014) 2081–2087.
[15] J.Y. Pastor, J. Llorca, A. Martín, J.I. Peña, P.B. Oliete, J. Eur. Ceram. Soc. 28 (2008) 2345–2351.
[16] H. Su, J. Zhang, K. Song, L. Liu, H. Fu, J. Eur. Ceram. Soc. 31 (2011) 1233–1239.
[17] D.-Y. Park, J.-M. Yang, Mater. Sci. Eng. A 332 (2002) 276–284.
[18] J. LLorca, J.Y. Pastor, P. Poza, J.I. Pena, I. de Francisco, A. Larrea, V.M. Orera, J. Am. Ceram. Soc. 84 (2004) 633–639.
[19] J. Llorca, V. Orera, Prog. Mater. Sci. 51 (2006) 711–809.
[20] N.R. Harlan, R.I. Merino, J.I. Pena, J. Am. Ceram. Soc. 85 (2002) 2025–2032.
[21] I. de Francisco, R.I. Merino, V.M. Orera, A. Larrea, J.I. Peña, J. Eur. Ceram. Soc. 25 (2005) 1341–1350.
[22] S.C. Farmer, A. Sayir, Eng. Fract. Mech. 69 (2002) 1015–1024.
[23] A. Laidoune, K. Lebbou, D. Bahloul, J. Cryst. Growth 380 (2013) 224–227.
[24] J.H. Lee, A. Yoshikawa, H. Kaiden, K. Lebbou, T. Fukuda, D.H. Yoon, Y. Waku, J. Cryst. Growth 231 (2001) 179–185.
[25] S.M. Lakiza, L.M. Lopato, J. Am. Ceram. Soc. 80 (1997) 893–902.
[26] J.Y. Pastor, J. Llorca, P. Poza, I. de Francisco, R.I. Merino, J.I. Peña, J. Eur. Ceram. Soc. 25 (2005) 1215–1223.
[27] T. Nagira, H. Yasuda, S. Takeshima, T. Sakimura, Y. Waku, K. Uesugi, J. Cryst. Growth 311 (2009) 3765–3770.
[28] W.A. Tiller, K.A. Jackson, J.W. Rutter, B. Chalmers, Acta Metall. 1 (1953) 428–437.
[29] J.H. Lee, A. Yoshikawa, S.D. Durbin, D. Ho Yoon, T. Fukuda, Y. Waku, J. Cryst. Growth 222 (2001) 791–796.
[30] S. Bourban, N. Karapatis, H. Hofmann, W. Kurz, Acta Mater. 45 (1997) 5069–5075.
[31] V.S. Stubican, R.C. Hink, S.P. Ray, J. Am. Ceram. Soc. 61 (1978) 17–21.
[32] J.I. Peña, R.I. Merino, N.R. Harlan, A. Larrea, G.F. de la Fuente, V.M. Orera, J. Eur. Ceram. Soc. 22 (2002) 2595–2602.